Supporting Information for

Aqueous All-Manganese Batteries

*Mingming Wang†, Yahan Meng†, Yan Xu, Na Chen, Mingyan Chuai, Yuan Yuan, Jifei Sun, Zaichun Liu, Xinhua Zheng, Ziqi Zhang, Dongjun Li, Wei Chen**

Department of Applied Chemistry, School of Chemistry and Materials Science, Hefei National Research Center for Physical Sciences at the Microscale, University of Science and Technology of China, Hefei, Anhui 230026, China

**Corresponding authors: weichen1@ustc.edu.cn*

Experimental

Materials.

The chemicals and materials in this work are all commercially available and used as received: manganese sulfate monohydrate ($MnSO_4 \cdot H_2O$, Sinopharm Chemical Reagent Co., Ltd), manganese chloride tetrahydrate ($MnCl_2 \cdot 4H_2O$, Sigma Aldrich), manganese nitrate solution ($Mn(NO_3)_2$, Sinopharm Chemical Reagent Co., Ltd), selenium dioxide (SeO_2, Sigma Aldrich), zinc sulfate heptahydrate ($ZnSO_4 \cdot 7H_2O$, Sinopharm Chemical Reagent Co., Ltd), copper sulfate pentahydrate ($CuSO_4 \cdot 5H_2O$, Sinopharm Chemical Reagent Co., Ltd), iron sulfate heptahydrate ($FeSO_4 \cdot 7H_2O$, Sinopharm Chemical Reagent Co., Ltd), ammonium sulfate ($(NH_4)_2SO_4$, Sigma Aldrich), ammonium chloride (NH_4Cl, Sigma Aldrich), sulfuric acid (H_2SO_4, Sinopharm Chemical Reagent Co., Ltd), carbon cloth (thickness of 200 μm, Fuel Cell Store, USA), Cu foil (thickness of 100 μm, Sinopharm Chemical Reagent Co., Ltd), carbon felt (Dalian Longtian Tech. Co.), graphite rod (Alfa Aesar, 99.9995%) and deionized water (resistance of 18.2 MΩ, Milli Q).

Characterizations.

Scanning electron microscope (SEM, Hitachi 8220, Japan) was carried out to characterize the morphologies and structures of the electrodes. Transmission electron microscopy (TEM), high-resolution TEM (HRTEM) images and energy dispersive X-ray spectra (EDS) of the samples were collected on JEM F200 electron microscope at an acceleration voltage of 100 kV. X-ray photoelectron spectroscopy (Thermo ESCALAB 250Xi) was performed with Al K_α source. X-ray diffraction (XRD) patterns were collected on a Philips X'Pert PRO SUPER X-ray diffractometer equipped with graphite monochromatized Cu K_α radiation. Mn L-edge XAS and some related XPS tests were performed at the Photoelectron Spectroscopy Terminal Station on beamline BL10B at the National Synchrotron Radiation Laboratory (NSRL) in Hefei, China.

Electrochemical tests.

The battery cycling performance was tested on battery test systems (LandHe, Wuhan, China, and Neware, Shenzhen, China). The galvanostatic charge-discharge rate capability and cyclic voltammetry of the three-electrode systems were carried out on a VMP3 electrochemical workstation (Bio-Logic, France). In the three-electrode measurements, metal foil, graphite rod and Ag/AgCl were used as the working, counter and reference electrodes, respectively. In the two-electrode symmetric battery, two metal foils were used as the working, counter and reference electrodes. The electrolyte composition of SeO_2-free $MnSO_4$ is 1 mol L^{-1} $MnSO_4$ and 1 mol L^{-1} $(NH_4)_2SO_4$. The electrolyte composition of SeO_2-additive $MnSO_4$ is 1 mol L^{-1} $MnSO_4$, 1 mol L^{-1} $(NH_4)_2SO_4$ and 0.02 g L^{-1} SeO_2. In the fabrication of the two-electrode full cell, carbon felts and Mn foil were acting as the cathode and anode, respectively, and the electrolyte consists of 1 mol L^{-1} $MnSO_4$, 1 mol L^{-1} $(NH_4)_2SO_4$, 0.02 g L^{-1} SeO_2, and 0.05 mol L^{-1} H_2SO_4 in water. The list of pH values of different electrolytes is shown in Table S2. All electrochemical tests were conducted at room temperature (~ 25 ℃).

The detailed calculation of theoretical capacity and energy density of the aqueous all-Mn battery.

When calculating the theoretical energy density, only the active materials of the positive and negative electrodes are considered, and the mass of other components is not considered. Therefore, the theoretical energy density calculation formula is as follows:

$$C_{(\text{battery specific capacity})}=1/(1/C_{(\text{cathode specific capacity})}+1/C_{(\text{anode specific capacity})})$$

$$E_{(\text{theoretical energy density})} = C_{(\text{battery specific capacity})} * V_{(\text{average discharge voltage})}$$

It is known that the theoretical specific capacity of the cathode MnO_2/Mn^{2+} is 616 mAh g^{-1}, and that of the anode Mn^{2+}/Mn is 976 mAh g^{-1}. Therefore, the theoretical energy density of the aqueous all-Mn battery is calculated as follows:

$$C_{(\text{battery specific capacity})}=1/(1/616+1/976)=377.65 \text{ mAh } g^{-1}$$

$$E_{(\text{theoretical energy density})} = 377.65 \text{ mAh } g^{-1} * 2.42 \text{ V}=913 \text{ Wh } kg^{-1}$$

	Cu	Fe	Zn	Al	Mg	Ca	K	Na	Li	Mn
M^{x+} cation radius (pm)	87	78	74	53.5	72	100	138	102	76	83
Volumetric capacity (mAh cm^{-3})	7558	7558	5854	2980	3833	2077	592	1128	2061	7250
Specific capacity (mAh g^{-1})	843	960	820	8035	2205	1340	687	1166	3860	976
Price ($ ton^{-1})	9451	60	2944	2510	3000	1000	1470	8900	16500	2000
M^{x+}/M redox potential vs SHE (V)	+0.34	-0.44	-0.76	-1.67	-2.37	-2.87	-2.92	-2.71	-3.04	-1.18

Table S1. Comparison of the properties of different metal electrodes.

Solutions	1 mol L^{-1} $MnSO_4$	1 mol L^{-1} $MnSO_4$+ 1 mol L^{-1} $(NH_4)_2SO_4$	1 mol L^{-1} $MnSO_4$+ 1 mol L^{-1} $(NH_4)_2SO_4$+Se	1 mol L^{-1} $MnCl_2$	1 mol L^{-1} $MnCl_2$+ 1 mol L^{-1} NH_4Cl	1 mol L^{-1} $Mn(NO_3)_2$	1 mol L^{-1} $Mn(NO_3)_2$+ 1 mol L^{-1} NH_4Cl
1st	2.88	3.56	3.47	2.64	3.63	0.76	1.53
2nd	2.89	3.51	3.48	2.58	3.66	0.81	1.55
3rd	2.89	3.52	3.44	2.56	3.71	0.81	1.49
Average pH	2.887	3.53	3.463	2.593	3.667	0.793	1.523

Table S2. The list of pH values of different electrolytes in this work.

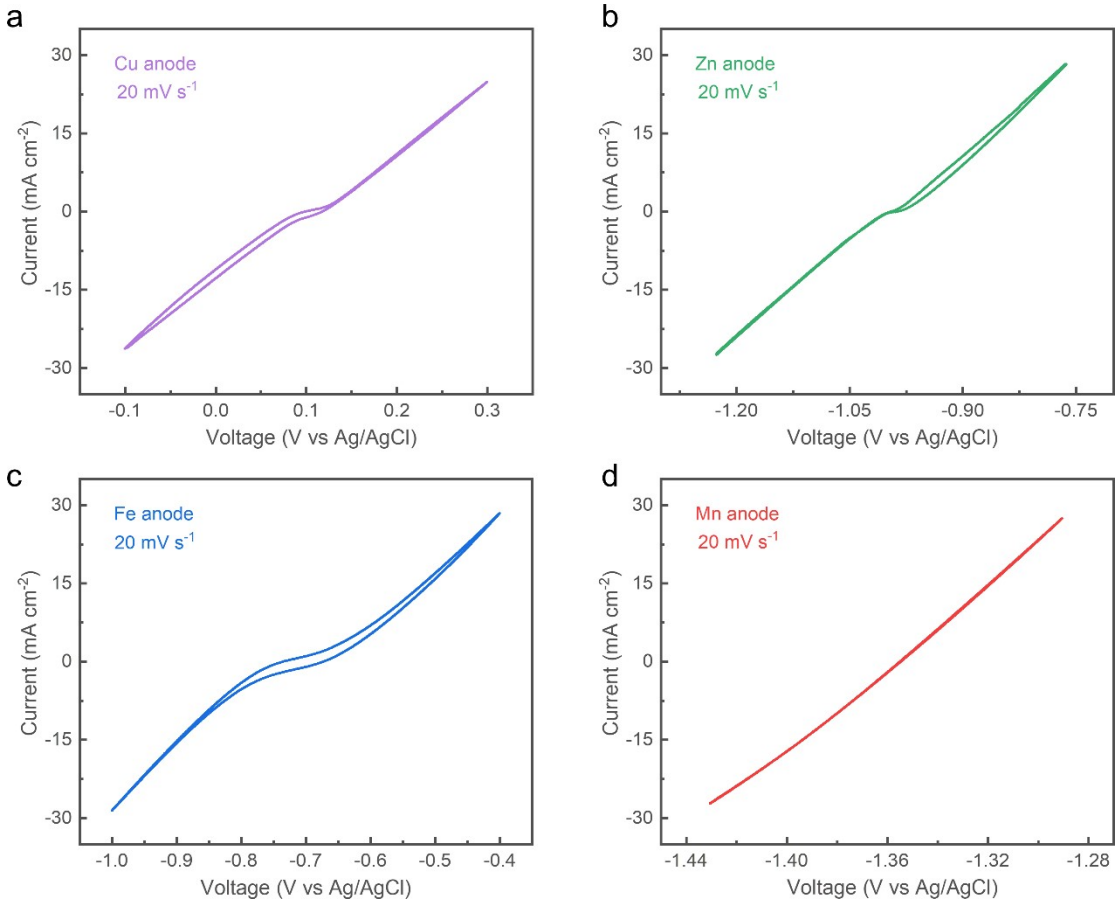

Figure S1. CV curves of Cu, Zn, Fe and Mn anodes in aqueous electrolytes at a scan rate of 20 mV s^{-1}. The tests were performed in a three-electrode system using metal foil, graphite rod, and Ag/AgCl electrode as working electrode, counter electrode, and reference electrode, respectively. The corresponding electrolyte is 1 mol L^{-1} metal sulfate in water.

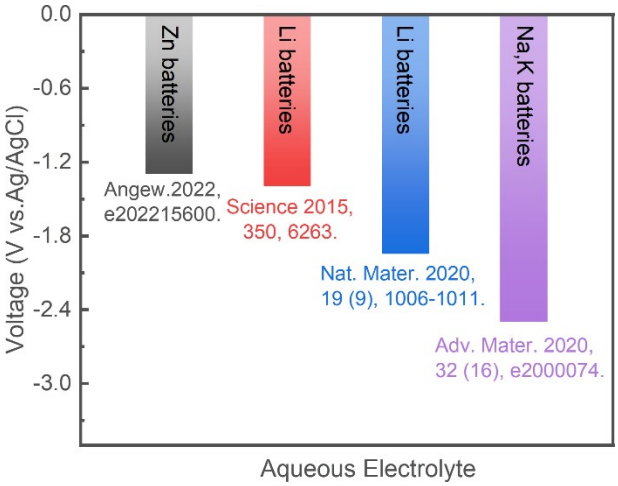

Figure S2. Summary of working potentials of aqueous batteries from some representative literature.

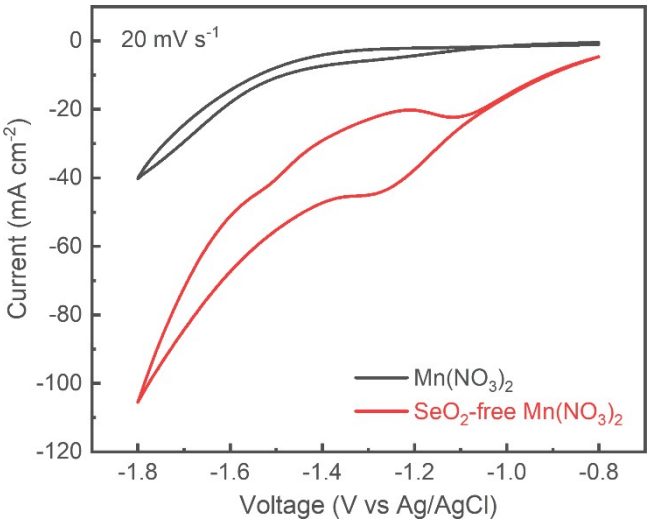

Figure S3. CV comparison in different $Mn(NO_3)_2$ based aqueous electrolytes. The tests were conducted in a three-electrode system using Mn foil, graphite rod, and Ag/AgCl electrode as working electrode, counter electrode, and reference electrode, respectively, in $Mn(NO_3)_2$ and SeO_2-free $Mn(NO_3)_2$ electrolytes.

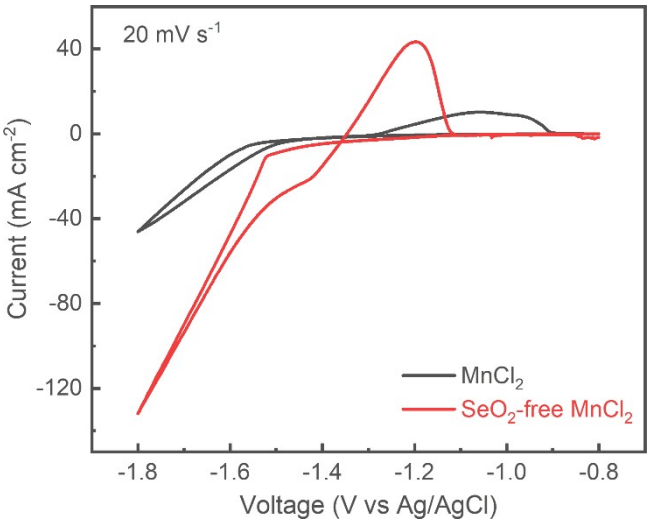

Figure S4. CV comparison in different $MnCl_2$ based aqueous electrolytes. The tests were conducted in a three-electrode system using Mn foil, graphite rod, and Ag/AgCl electrode as working electrode, counter electrode, and reference electrode, respectively, in $MnCl_2$ and SeO_2-free MnCl electrolytes.

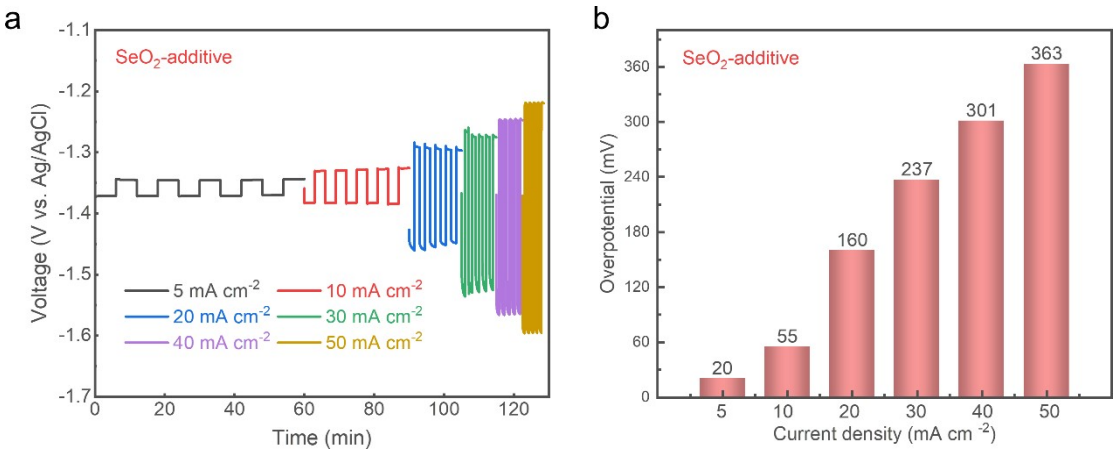

Figure S5. (a) Galvanostatic charge-discharge tests of a three-electrode cell for Mn anode in SeO_2-additive $MnSO_4$ electrolyte, where the working, counter, and reference electrodes are Mn foil, graphite rod and Ag/AgCl, respectively. (b) Summary of the Mn anode overpotentials under different current densities.

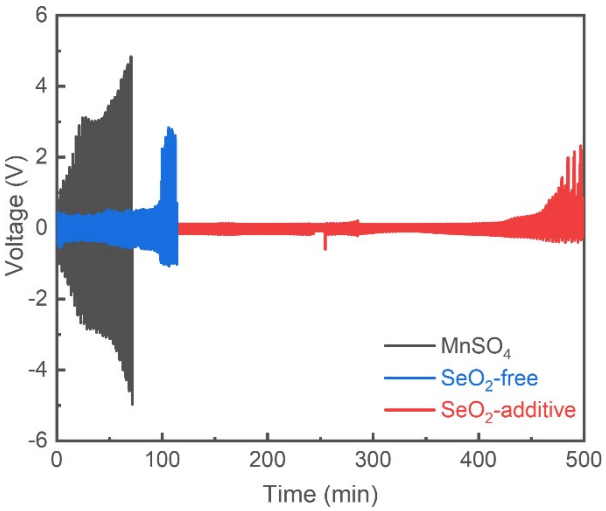

Figure S6. Cycling curves of Mn-Mn symmetric batteries in different electrolytes.

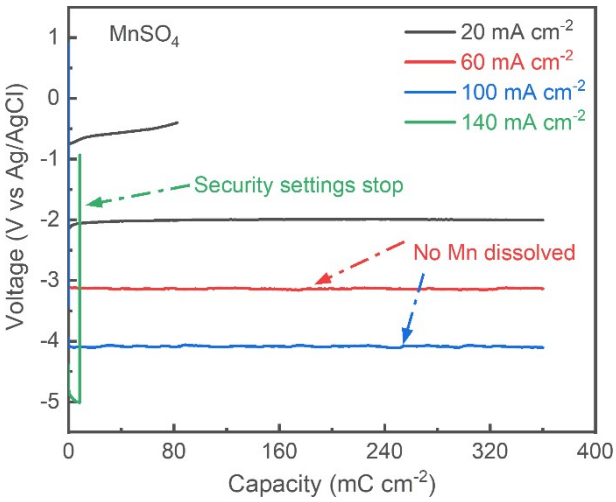

Figure S7. Galvanostatic charge-discharge tests of Cu|Mn asymmetric half-cell in $MnSO_4$ electrolyte.

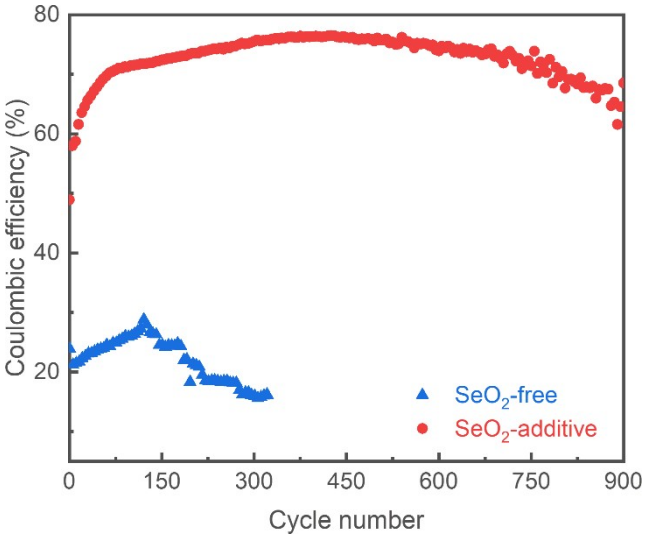

Figure S8. The CE of Mn deposition and dissolution cycles in different electrolytes.

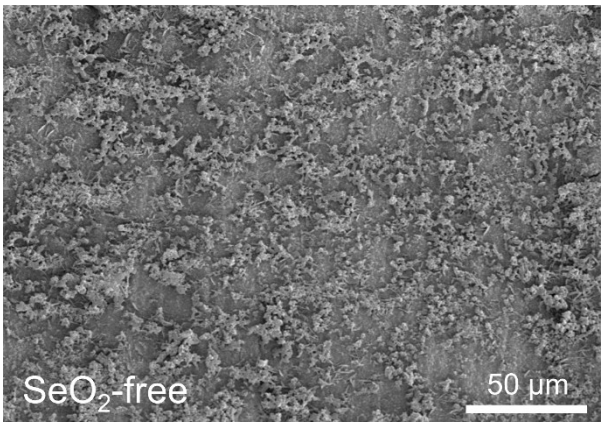

Figure S9. SEM image of deposited Mn in SeO_2-free $MnSO_4$ electrolyte.

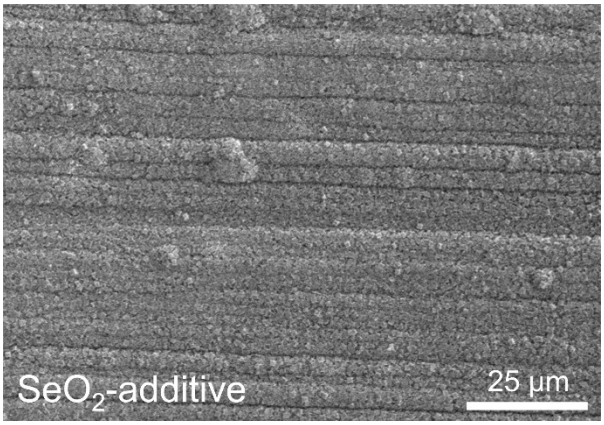

Figure S10. SEM image of deposited Mn in SeO_2-additive $MnSO_4$ electrolyte.

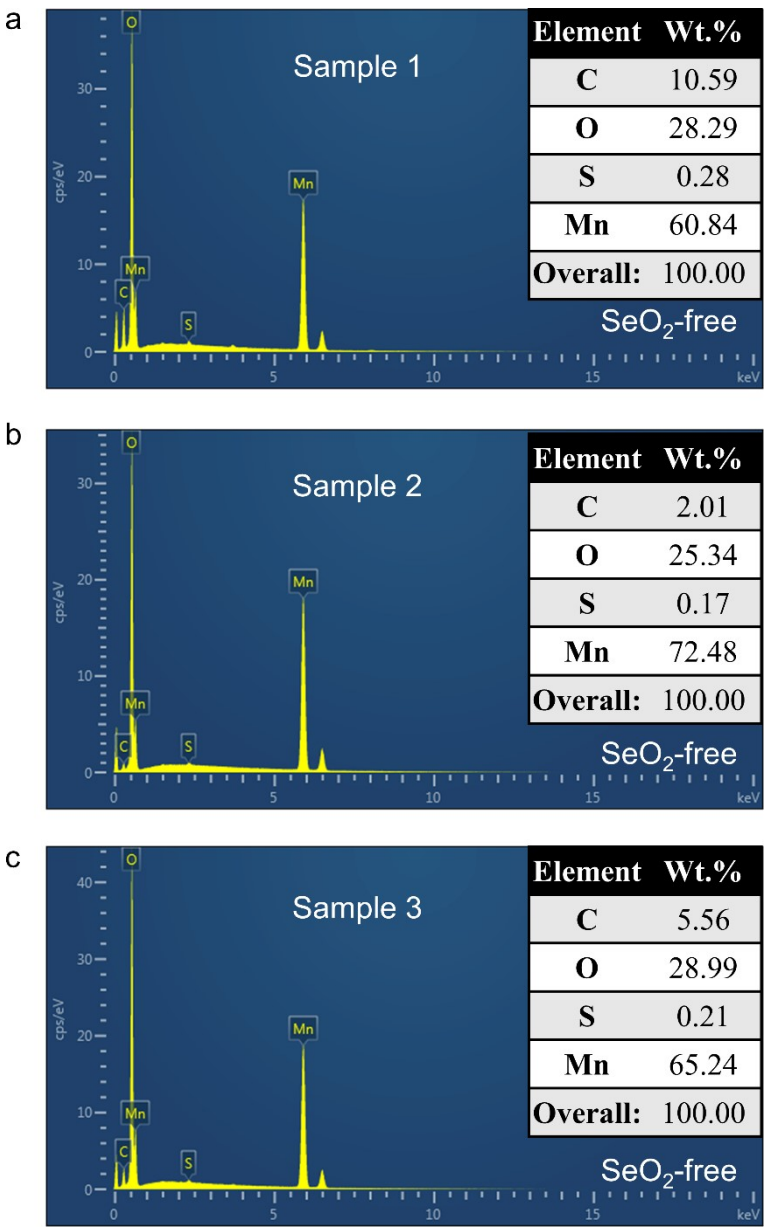

Figure S11. EDS spectra of deposited Mn on Cu foil in SeO_2-free $MnSO_4$ electrolyte. The table in the figure shows the content of different elements.

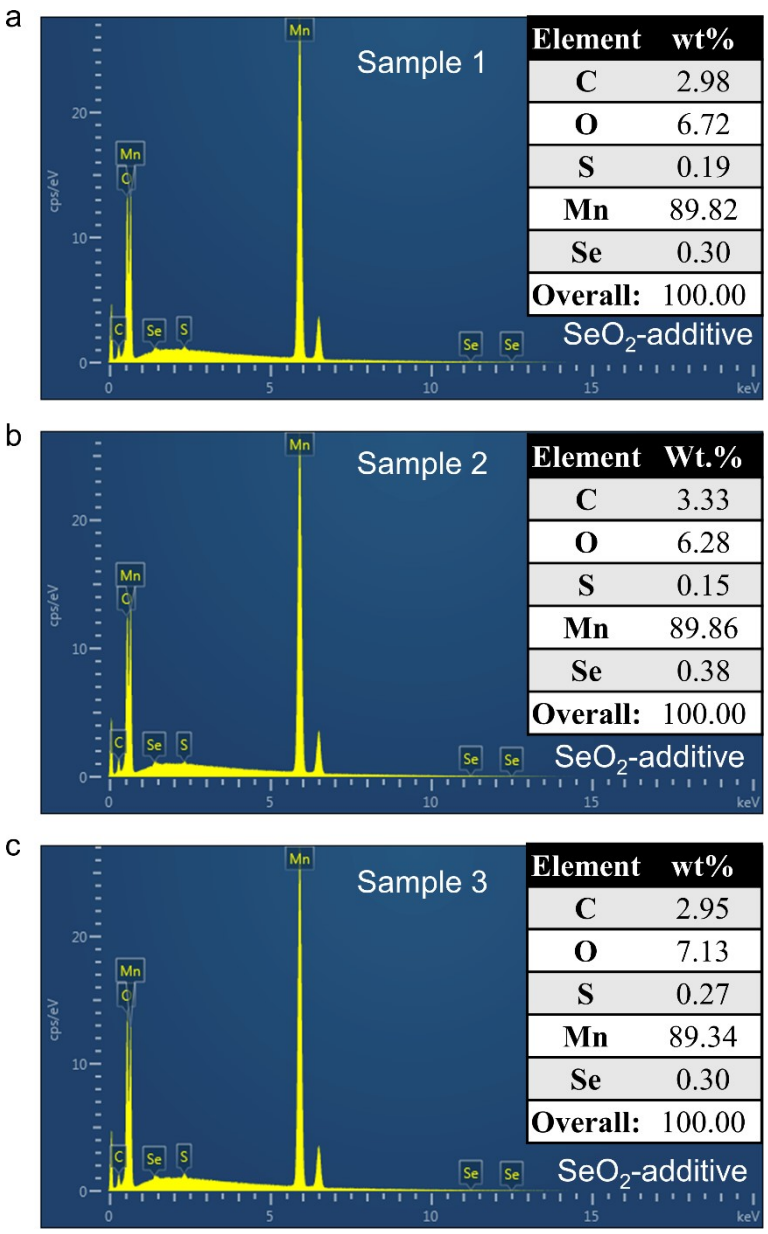

Figure S12. EDS spectra of deposited Mn on Cu foil in SeO_2-additive $MnSO_4$ electrolyte. The table in the figure shows the contents of different elements.

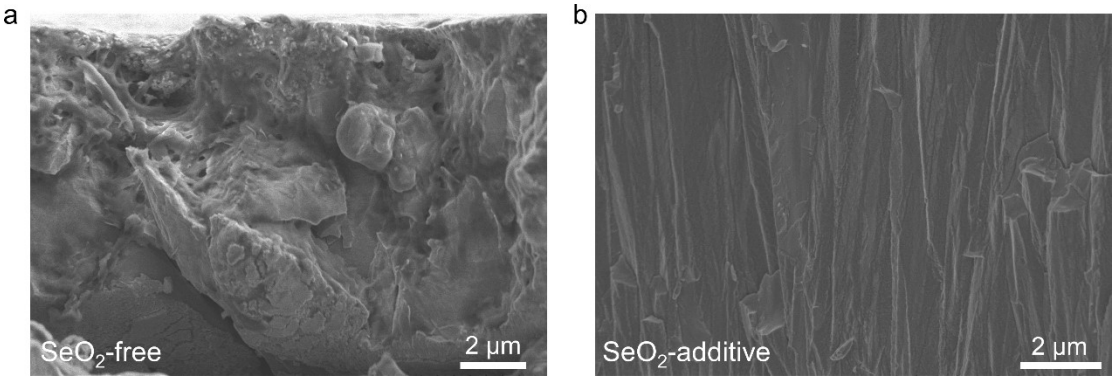

Figure S13. Cross-sectional SEM images of deposited Mn in SeO_2-free $MnSO_4$ electrolyte (a) and SeO_2-additive $MnSO_4$ electrolyte (b).

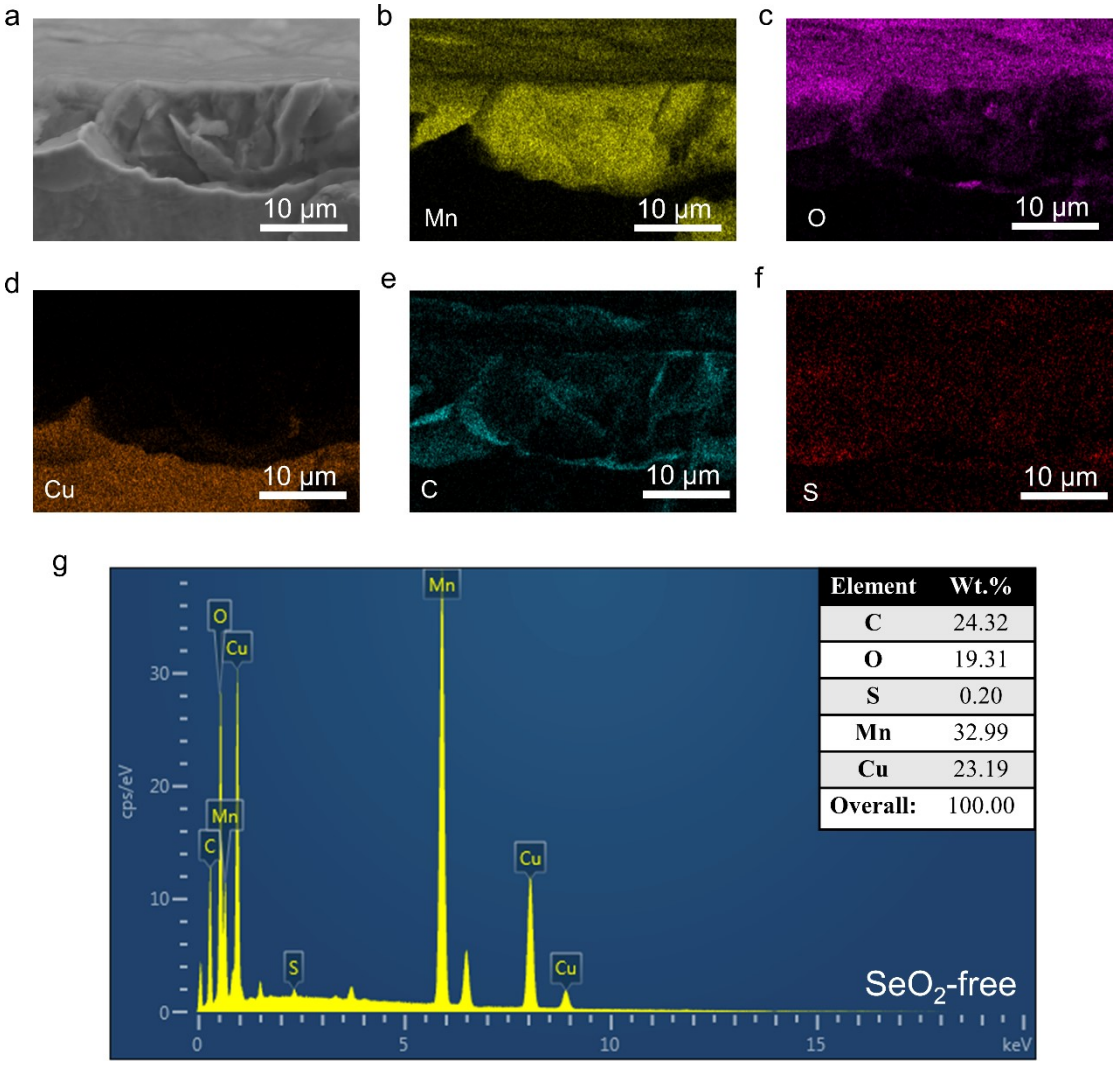

Figure S14. EDS mapping of cross-section of deposited Mn on Cu foil in SeO_2-free $MnSO_4$ electrolyte. The table in the figure shows the contents of different elements.

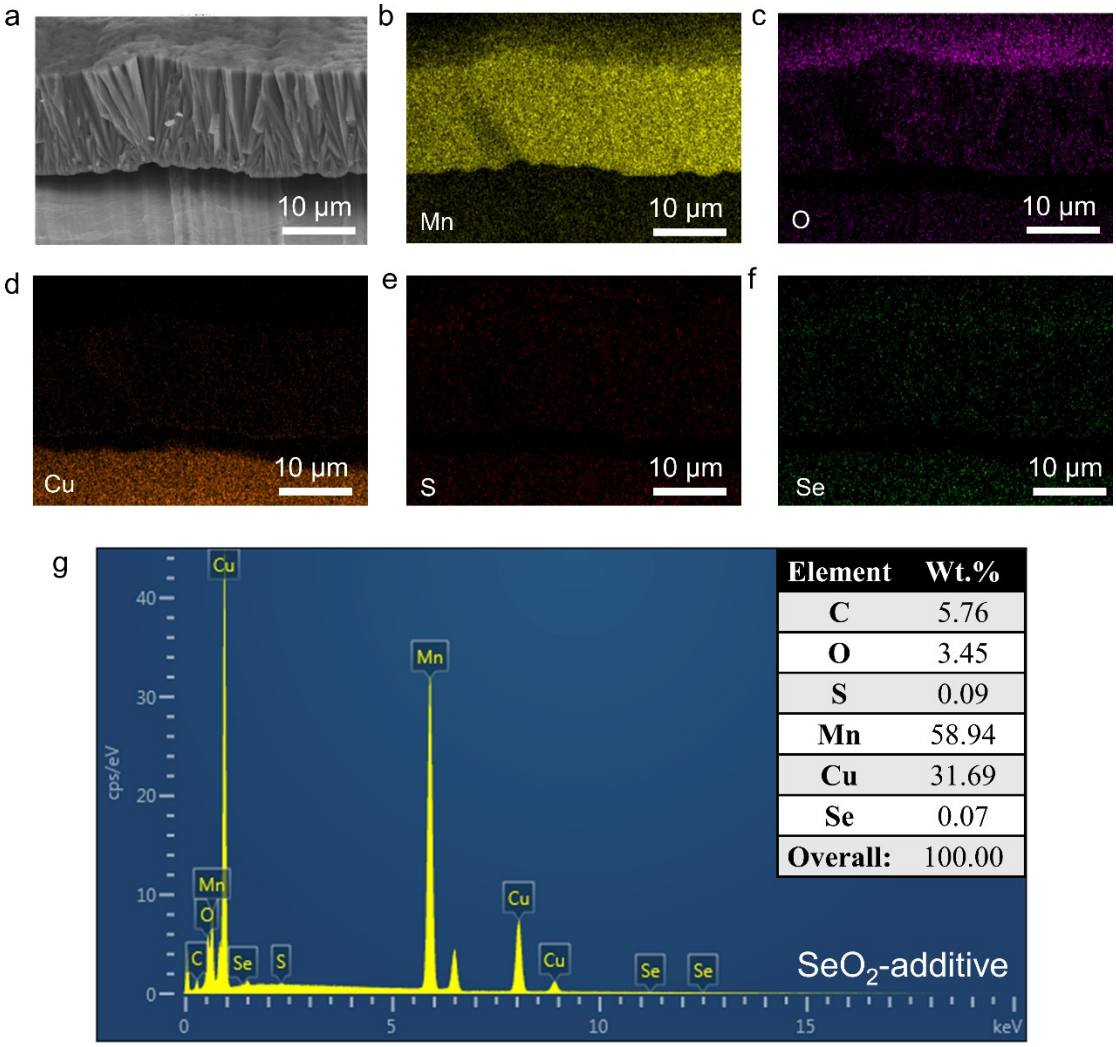

Element	Wt.%
C	5.76
O	3.45
S	0.09
Mn	58.94
Cu	31.69
Se	0.07
Overall:	100.00

Figure S15. EDS mapping of cross-section of deposited Mn on Cu foil in SeO_2-additive $MnSO_4$ electrolyte. The table in the figure shows the contents of different elements.

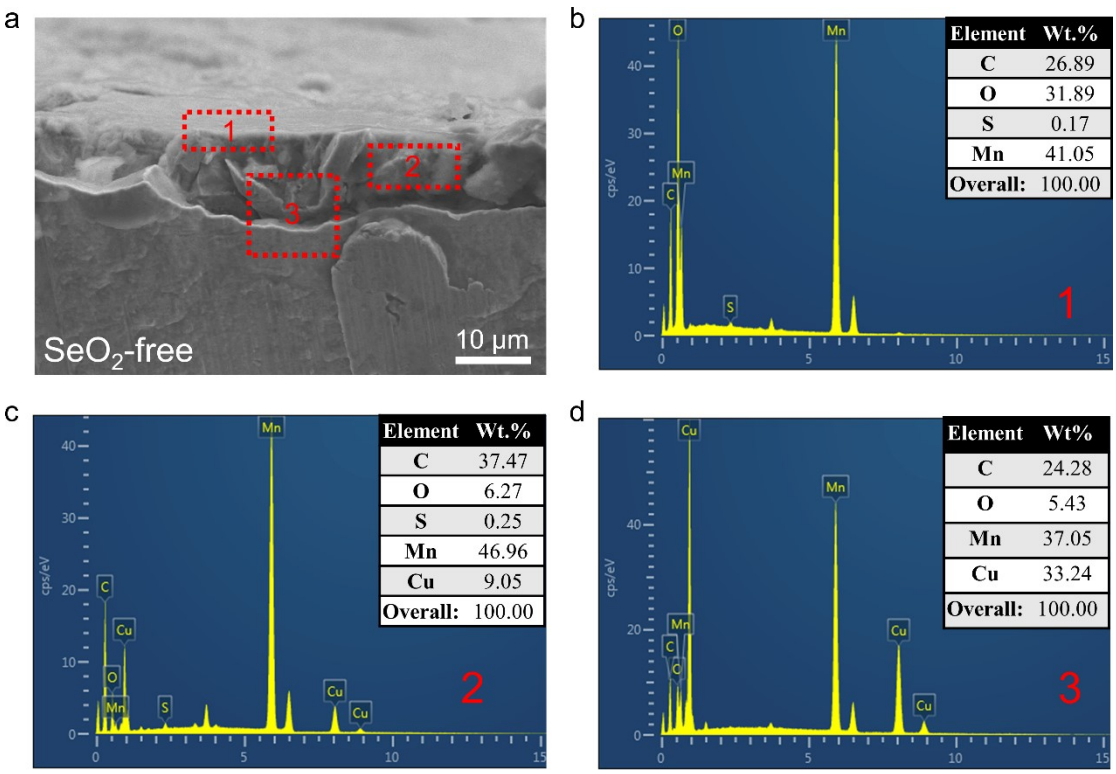

Figure S16. Point scan EDS mapping of different areas of deposited Mn on Cu foil in SeO_2-free $MnSO_4$ electrolyte. The table in the figure shows the contents of different elements.

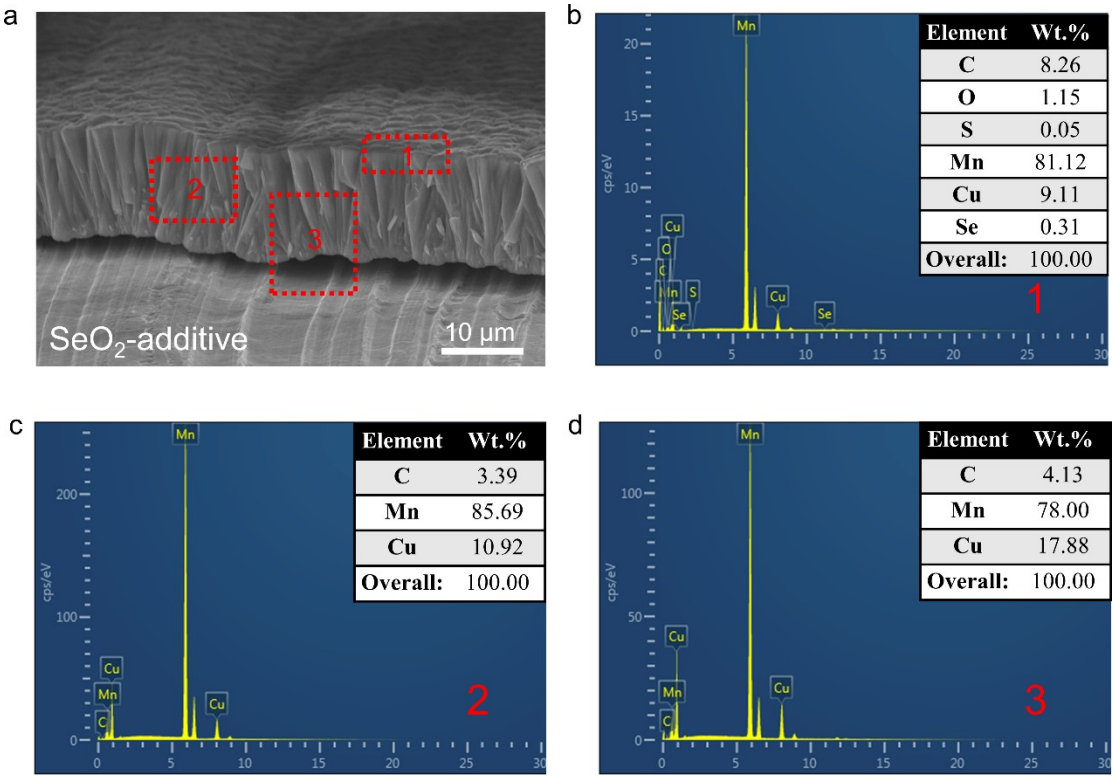

Figure S17. Point scan EDS mapping of different areas of deposited Mn on Cu foil in SeO_2-additive $MnSO_4$ electrolyte. The table in the figure shows the contents of different elements.

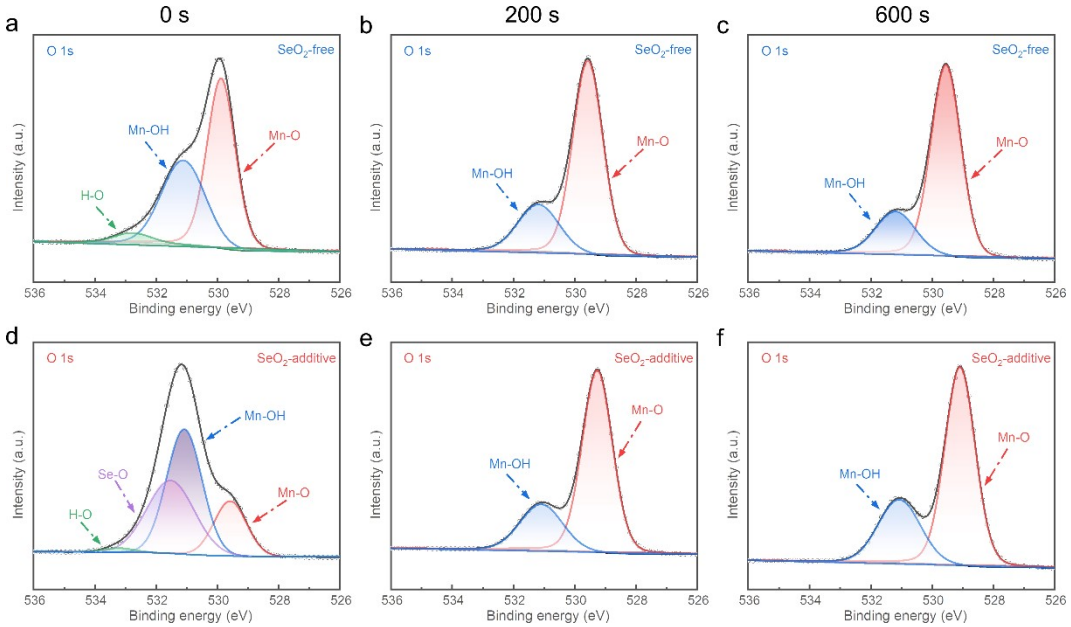

Figure S18. XPS of O 1s of deposited Mn on Cu foil in SeO_2-free $MnSO_4$ electrolyte (a-c) and SeO_2-additive $MnSO_4$ electrolyte (d-e) after Ar^+ sputtering for different durations: (a, d) 0 s, (b, e) 200 s, (c, f) 600 s.

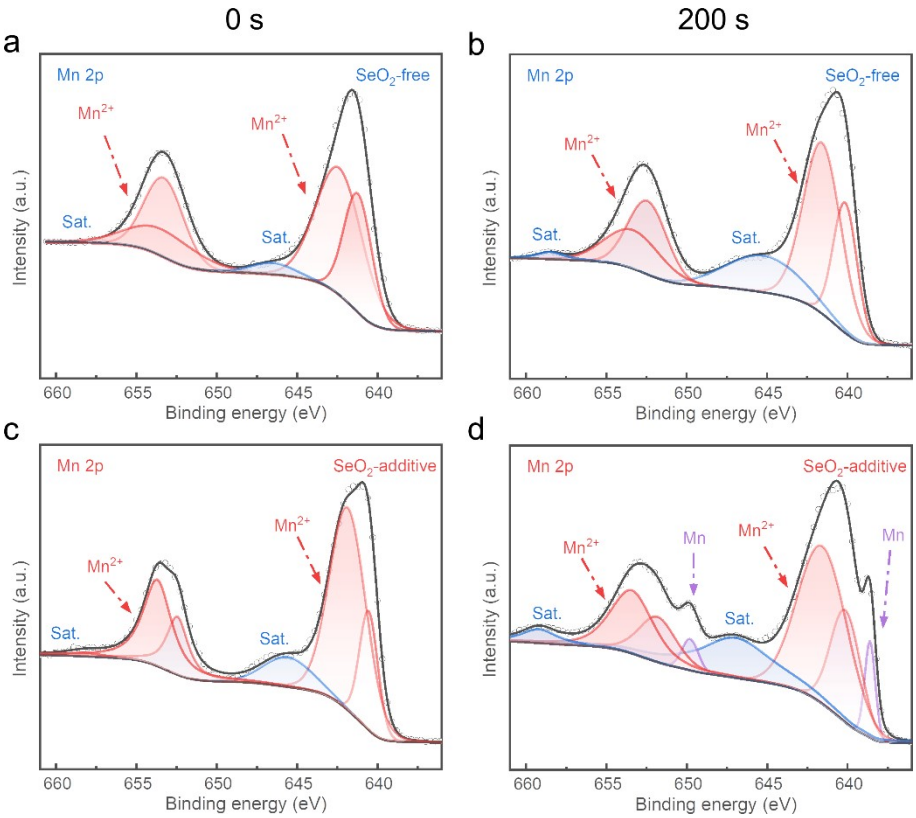

Figure S19. XPS of Mn 2p of deposited Mn on Cu foil in SeO_2-free $MnSO_4$ electrolyte (a-b) and SeO_2-additive $MnSO_4$ electrolyte (c-d) after Ar^+ sputtering for different durations: (a, c) 0 s, (b, d) 200 s.

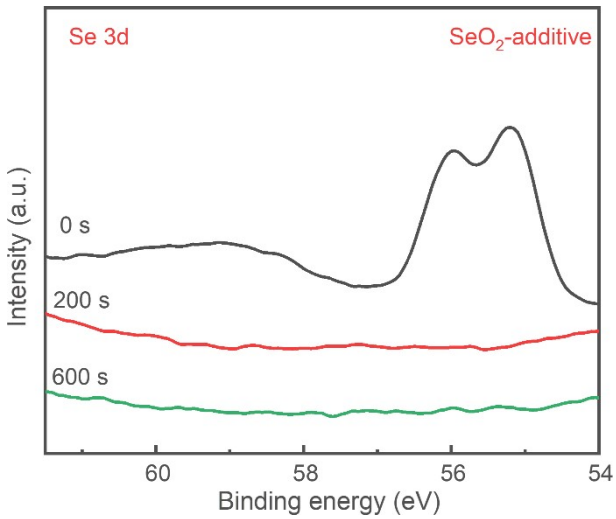

Figure S20. XPS of Se 3d of deposited Mn on Cu foil in SeO_2-additive $MnSO_4$ electrolyte after Ar^+ sputtering for different durations.

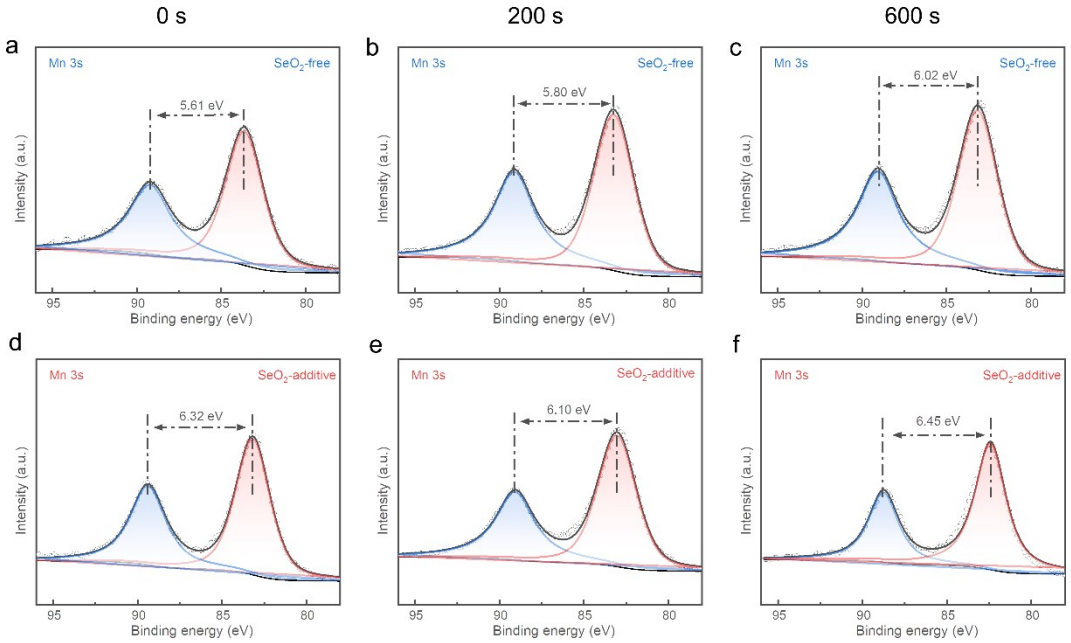

Figure S21. XPS of Mn 3s of deposited Mn on Cu foil in SeO_2-free $MnSO_4$ electrolyte (a-c) and SeO_2-additive $MnSO_4$ electrolyte (d-e) after Ar^+ sputtering for different durations: (a, d) 0 s, (b, e) 200 s, (c, f) 600 s.

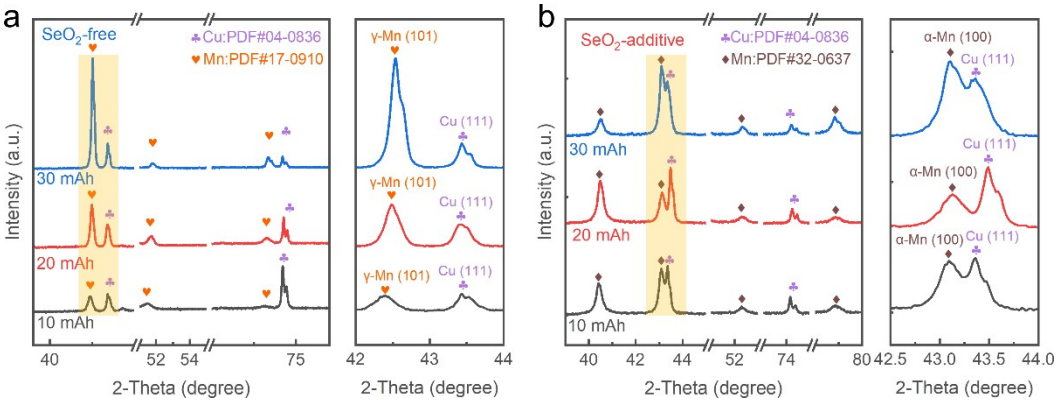

Figure S22. XRD of deposited Mn on Cu foil with different capacities in different electrolytes.

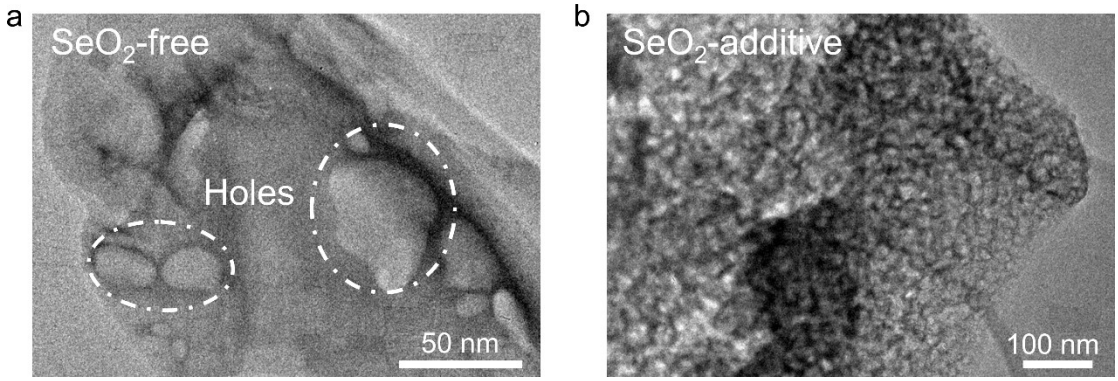

Figure S23. TEM images of deposited Mn in SeO_2-free (a) and SeO_2-additive $MnSO_4$ electrolytes (b).

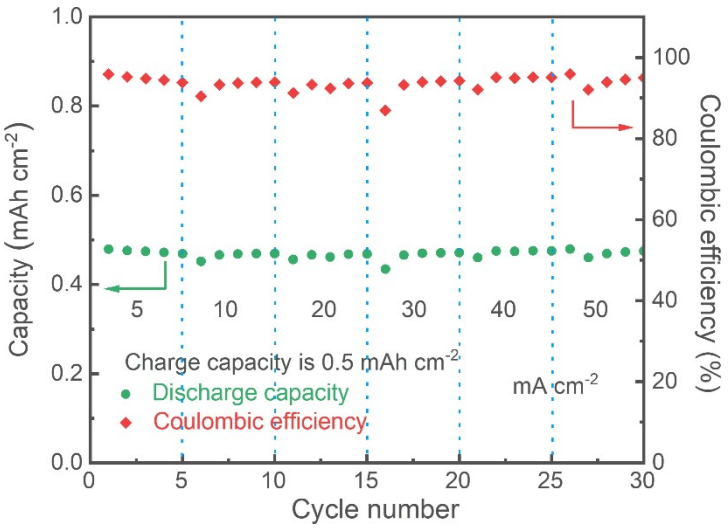

Figure S24. Rate performance of AAMB with different current densities from 5 to 50 mA cm^{-2}.

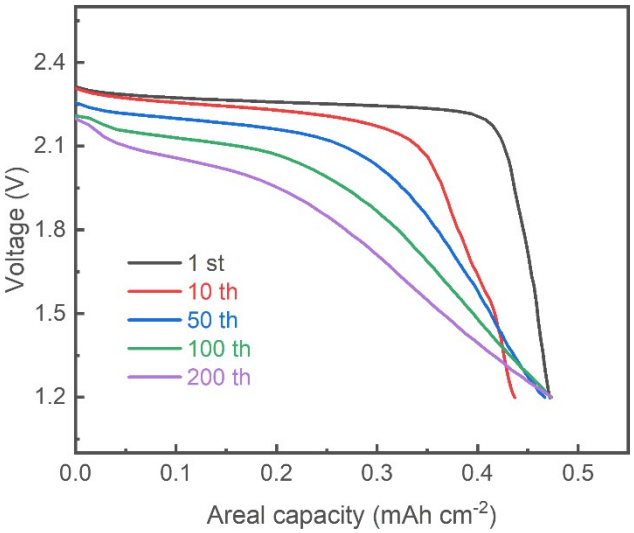

Figure S25. Discharge curves of aqueous all-Mn batteries in different cycles.

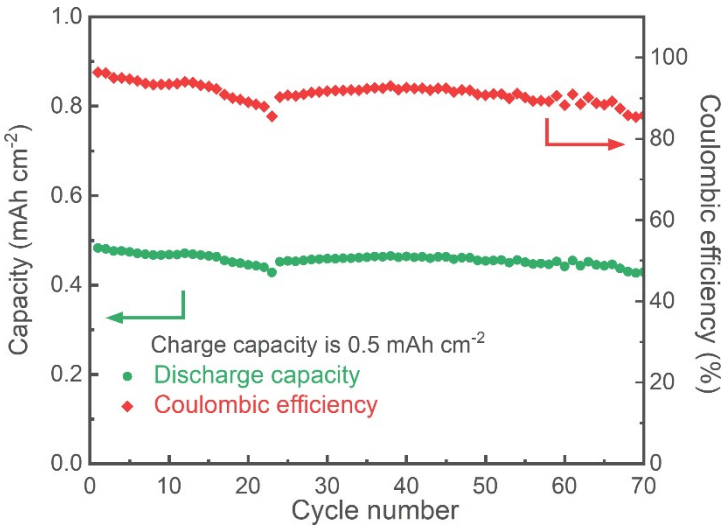

Figure S26. Cycling test of AAMB at 2 mA cm^{-2}.

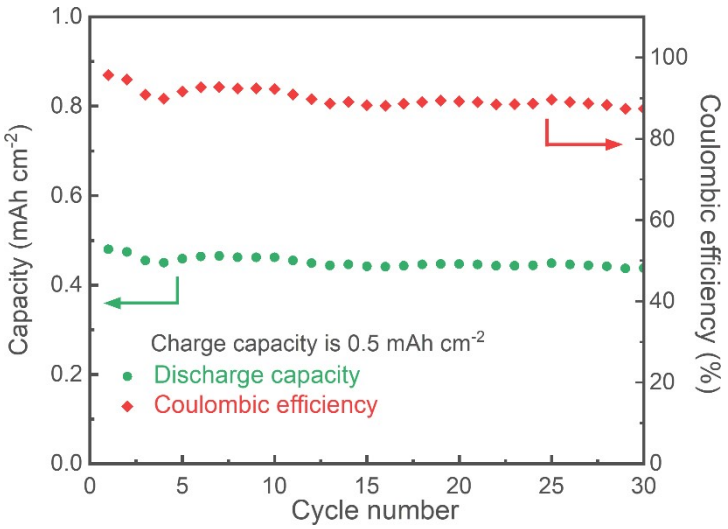

Figure S27. Cycling test of AAMB at 1 mA cm^{-2}.

Figure S28. A digital photograph of an LED screen with the logo of “USTC” lighting by the AAMB.

Battery type	Electrochemical reaction mechanism	Work Voltage (V)	Theoretical energy density (Wh kg^{-1})	Practical energy density (Wh kg^{-1})	Status
Aqueous all-Mn battery	$Mn + MnO_2 + 2H_2SO_4 \leftrightarrow 2M$	2.42	913	-	Proof-of-concept
Organic Li-ion battery	$LiC_6 + FePO_4 \leftrightarrow LiFeO_4 + 6C$	3.3	385	150	Mature commercialization
Aqueous Lead-acid battery	$Pb + PbO_2 + 2H_2SO_4 \leftrightarrow 2PbS$	2.0	167	35	Mature commercialization
Aqueous Ni-Fe battery	$Fe + 2NiOOH + 2H_2O \leftrightarrow Fe($	1.2	234	40	Mature commercialization
Aqueous Ni-MH battery	$MH + NiOOH \leftrightarrow M + Ni(OH)$	1.35	340	100	Mature commercialization
Aqueous Alkaline-Ni-Zn battery	$Zn + 2NiOOH + 2H_2O \leftrightarrow Zn($	1.7	372	90	Mature commercialization
Aqueous All-V flow battery	$VO_2^+ + V^{2+} + 2H^+ \leftrightarrow VO^{2+}$	1.26	250	<50	Mature commercialization
HT Na-S battery	$2Na + xS \leftrightarrow Na_2S_x$	~2	760	-	Mature commercialization
Organic Na-ion battery	$Na_xC_6 + Na_{1-x}MO_2 \leftrightarrow NaM($	2~4	300~400	100	Under development
Aqueous Na-ion battery	$2Na_3MnTi(PO_4)_3 \leftrightarrow Na_4MnT$	1.4	41	-	Under development
Aqueous K-ion battery	$KFeMnHCF + PCTDI \leftrightarrow K_xP$	1.2	-	-	Under development
Aqueous Al-ion battery	$Al_xMnO_2 \cdot nH_2O + (y-x)Al$	1.1	561	-	Under development
Aqueous Zn-ion	$Zn + 2MnO_2 \leftrightarrow ZnMn_2O_4; Zn$	1.35	302	-	Under development

battery	$1.1Zn + Zn_{0.25}V_2O_6 \leftrightarrow Zn_{1.35}V$	0.8	175	-	Under development

Table S3. Comparison of different commercialized electrochemical energy storage technologies and other aqueous batteries.

Movie S1. Mn plating and stripping in SeO_2-additive $MnSO_4$ electrolyte.